RESEARCH PAPER

Investigation of stress relief crack susceptibility of CrMoV steels coarse grain HAZ via simulation of uniaxial stress conditions during PWHT

D. Czeskleba[1] · J. Nietzke[1] · M. Rhode[1,2] · T. Kannengiesser[1,2]

Abstract

Creep-resistant steels such as the 13CrMoV9-10, used in the construction of thick-walled pressure vessels, are most commonly submerged arc welded (SAW). These steels can develop stress relief cracks (SRC) if the mandatory post weld heat treatment (PWHT) is performed improperly. Current PWHT parameters, such as heating rate and holding time at a specific holding temperature, are based on both empirical experience and conventional free shrinking welding experiments to characterize the SRC-susceptibility of the weld. These cannot adequately depict the higher residual stresses caused by the structurally induced stiffness of the surrounding construction.

This study discusses the development of a repeatable, precise, and time-efficient methodology to study the effects of different stress levels and heating rates on the SRC susceptibility of the coarse grain heat-affected zone (CGHAZ). For that purpose, samples were thermically treated to simulate a coarse grain heat-affected zone (CGHAZ) and subsequently exposed to representative levels of stress during the heating phase of a PWHT. The recorded stress and heating rate–dependent strains were mathematically analyzed via curve tracing/calculus to identify interdependent effects. This procedure facilitates the measurement of material characteristics such as carbide growth on grain boundaries at the μm-scale via an integrated value over the entire sample volume. The first and second derivatives show a slight, precipitate-dependent, increase in hardness of the sample, depending on the heating rate and applied stress. This new methodology generates an improved assessment of the SRC susceptibility of SAW microstructures of creep-resistant CrMoV steels.

Keywords Repair-welding · High-strength steels · Transient stresses · Residual stresses

1 Introduction

Modern creep-resistant and typically submerged arc-welded (SAW) steels such as the 13CrMoV9-10 show a comparatively high stress relief crack (SRC) susceptibility during construction. This stems from a complex combination and interaction of component specific, thermal, and metallurgic factors (Fig. 1) many of which have to date not been conclusively researched, such as the impact of the post weld heat treatments (PWHT) heating rate, in combination with

the influence of additional, global residual stresses and their constraint on the thermal shrinkage. These additional residual stresses stem from the component-specific, structurally induced stiffness and the high wall thicknesses required for industrial use in the petrochemical industry in deep desulfurization plants or hydrocracking units [1]. Together with metallurgic effects, especially due to the high heat input during the SAW process and the mandatory PWHT, such as hardening or carbide growth on the grain boundary, these factors combine to a very complex and interwoven field of variables (Fig. 1). Together, these lead to the high SRC susceptibility of the coarse grain heat-affected zone (CGHAZ) of the last weld bead during PWHT, which has been shown to be the critical area for the development of SRC [2–4].

Material thicknesses of up to 500 mm in modern applications and the structurally induced stiffness of the surrounding construction significantly impact the constraint on the thermal shrinkage of the weld. These constraints, together with the weld geometry and multiple passes
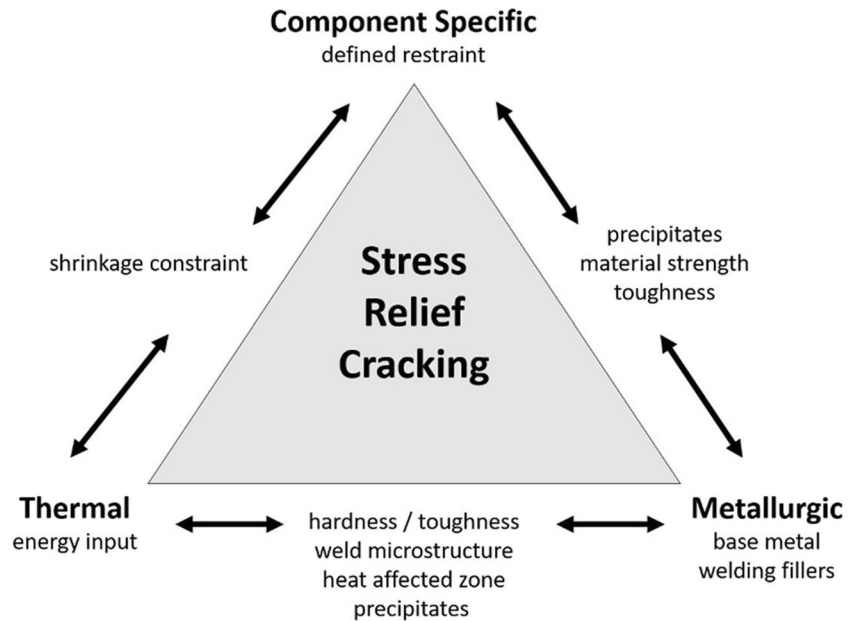
✉ D. Czeskleba
Denis.Czeskleba@BAM.de

1 Bundesanstalt fuer Materialforschung und -pruefung (BAM), Berlin, Germany

2 Otto-Von-Guericke University, Magdeburg, Germany

Fig. 1 SRC influencing factors of SAW welded joints, based on [5]

during the welding process, lead to a non-trivial, multiaxial global residual stress distribution including high levels of bending [2, 5].

SRCs develop during the PWHT due to the formation and growth of incoherent carbides on prior austenite grain boundaries, resulting in a significant hardness increase and toughness decrease [6, 7]. Microstructural changes due to different heating rates, or levels of stress present in the weld, as well as the identification of these highly localized precipitations on the μm-scale and their potential impact have not been observed via the use of scanning electron microscope (SEM) or transmission electron microscopy (TEM). Furthermore, traditional free-shrinking welding experiments or even self-constraining geometries with subsequent PWHT cycles can only be approximations of real stress conditions with limitations regarding accurate identification of the total stress present. Other studies, such as hot tensile tests commonly disregard the effect of the heating rate during PWHT.

The aim of this study was to develop an experimental methodology explicitly designed to include the additional (global) stresses and the heating rate and to allow for the analysis of the GCHAZ's properties and behavior during a PWHT on a macroscopic scale.

2 Materials and methods

The object of this study was the simulated CGHAZ of the 13CrMoV9-10 base material (BM), as the CGHAZ is the critical region for the occurrence of SRC [3, 4]. Adapted tensile test samples, in analogy to DIN EN ISO 6892–1, were extracted from 180-mm-thick BM. Table 1 shows the specific chemical composition, obtained via optical emission spectrometry (OES) for samples near the middle of the original thick sheet metal and within 60 mm of the top. The chemical differences were minute, hence for practicability; all samples were taken from the middle.

2.1 Sample geometry and CGHAZ simulation

The development of the sample geometry was driven by (a) the machinery used to conduct the experiments (TA Instruments Dilatometer DIL 805A/D) and its maximum allowable force (10 kN) and its screw fitting and (b) the length of the CGHAZ within the samples, governed by the induction field of the dilatometer. Uniformity of the CGAHZ in the gauge section was visually confirmed via etching and optical microscopy. An additional adaption of the classical tensile

Table 1 Chemical composition of base material (mass-%, rest Fe)

Method: Fe-30-N	Chemical composition [mass-%]												
	C	Si	Mn	P + S	B	Ca	Cr	Cu	Mo	N	Nb	Ni	V
Base metal (middle)	0.12	0.1	0.51	<0.016	0.0008	0.003	2.18	0.12	0.96	<0.040	0.031	0.15	0.32
Base metal (upper third)	0.12	0.1	0.5	<0.016	0.001	0.003	2.18	0.12	0.92	<0.040	0.028	0.15	0.3

test sample geometry in the form of a taper in the center of the sample was necessary to ensure the homogeneous distribution of the CGHAZ throughout the gauge section. This ensures the highest stress is in the critical area. The specific geometry which showed the best results, and was subsequently used, was samples with a length of 40 mm, a M5×5 fitting on both sides, and a 3.3-mm diameter outside the gauge section and a 2.5-mm diameter within.

The here discussed simulation was performed utilizing a TA Instruments Dilatometer DIL 805A/D in a nitrogen atmosphere. To simulate the CGHAZ, the samples were heated linearly with 50 K/s until the maximum temperature of 1350 °C was reached. During the subsequent cooling, an exponential cooling curve based on a $t_{8/5}$-time of 60 s was used. The cooling curve was modeled after data obtained via type K thermocouples from several free-shrinking SAW experiments of 25-mm-thick sheet metals with a heat input of 35 kJ/cm. This ensures a realistic CGHAZ. To ensure comparability with the cooling characteristics of the experimentally acquired temperature measurements and $t_{8/5}$-time, a thrice segmented cooling routine was utilized to match the real cooling curve as closely as practicably possible. A single heating and cooling cycle were performed to simulate the last weld beads CGHAZ.

2.2 Post weld heat treatment and stress level application

The same dilatometer setup was used during the application of the PWHT scenarios including the uniaxial stress application via a defined tension force. To evaluate the impact of the PWHT heating rate on the SRC susceptibility, three different heating rates (Φ in K/h) were chosen and applied from room temperature (RT) to 500 °C. A heating rate of $\Phi_1 = 33.3 K/h$ was defined as the lowest heating rate, $\Phi_2 = 100 K/h$ as the medium rate, and $\Phi_3 = 300 K/h$ as the high heating rate. A critical temperature window of 300–500 °C for the development of SRC had been identified in previous studies ([2, 8]); hence, the PWHT was stopped at 500 °C to identify the microstructural differences at that temperature.

Because of wall thicknesses of 500 + mm of the relevant real-world applications, and due to the rigidity of the surrounding structures, the weld seam is subject to very high multiaxial and design-dependent mechanical loads, so-called global stresses [9]. These global stresses were simplified to a very high uniaxial stress, which was then selectively applied during the experiments via a specific tension force setting. Used as the lower bound was 865 MPa for the utilized stress, 900 MPa for the medium level, and 1010 MPa for the high applied stress. Combinations of high and low stress levels with high and low heating rates respectively, as well as intermediate points between either extreme, were performed to examine their interactions (Table 2).

Table 2 Design of experiments

Stress heat input	33.3 K/h	100 K/h	300 K/h
865 MPa	X		X
900 MPa	X		
1010 MPa	X	X	X

After the CGHAZ simulation and a controlled cooling to 220 °C, the samples were allowed to cool freely to RT. As the samples reached the starting temperature of 25 °C, the required force was linearly applied until it reached the necessary force after 20 s. At which point the PWHT simulation, with specific heating rates, was initiated. During the heating of the sample, the force was held constant during the thermal expansion to allow for unhindered thermal expansion. The following test data was subsequently analyzed: temperature "T" in °C, the applied force "F" in N, the time "t" in s, and the length change of the sample "s" in mm.

2.3 Mathematical analysis

The motivation for the mathematical analysis of the length change over the temperature gradients is the need for an integrated value over the entire testing area of the sample correlated to the potentially critical temperature window. Minute local changes on the μm-scale are accumulated and combined into a detectable and easily repeatable and comparable value.

The recorded length needed to be correlated to the specific temperature at that time. Due to the TA Instruments Dilatometer DIL 805A/D also utilizing the recorded temperature as well as the force and length measurements for the internal process control, this could not be done directly. Instead, a monotonically non-decreasing time-dependent temperature gradient with equidistant basis points was applied based on the measured temperature data. This approach allows for a smoother and more reliable first derivative of the length change per degree Kelvin and decreases the necessary smoothing functions and filters. Thus, the notation in formula (1) and (2) is used, where the first derivative v_s can be thought of as the velocity of the length change per °K, and the second derivative a_s as the acceleration:

$$v_s = f'(T) = \frac{\Delta s}{\Delta T} \text{ First derivative } ("velocity"), \text{ unit}: \frac{mm}{K}$$
(1)

$$a_s = f''(T) = \frac{\Delta^2 s}{\Delta T^2} \text{ Second derivative } ("acceleration") \text{ unit}: \frac{mm}{K^2}$$
(2)

2.4 Correlation to established methodologies

To establish the viability of this new methodology, the results were correlated with established criterions for the

SRC susceptibility. Specifically, the hardness ([4, 10]) and visual differences in microstructure due to the variation of the mechanical load and heating rate were analyzed for this paper via Vickers hardness tests, optical analyses, and scanning electron microscopy (SEM).

The weld metal samples used for the hardness comparisons via Vickers hardness tests were extracted from a 40-mm-thick submerged arc weld, welded with one filler wire, 550 A and 30 V with positive polarization, a weld speed of 30 cm/min (33 kJ/cm) for the filler beads (9 layers, 2 beads each), and 50 cm/min (19.8 kJ/cm) for the root and top pass. The pre-heating temperature for the weld sample was 200 °C and the interpass temperature was 240 °C with a total weld length of 765 mm. The weld seam was prepared with a 0° angle and a welding gap of 20 mm. As filler material, a 4-mm Union S 1 CrMo 2 V wire and the agglomerated, fluoride basic type flux UV 430 TTR-W by voestalpine Böhler Welding GmbH was used. After welding, a dehydrogenation heat treatment (DHT) was performed at 350 °C for 4 h. The samples were extracted both lengthwise (along the weld seam) and crosswise (perpendicular to the weld seam) from pure weld metal.

The Vickers hardness tests were done via line scans (5 mm distance) in HV0.5 on a DuraScan 70G5 (EMCO-Test Prüfmaschinen GmbH) after a visual inspection via light microscopy on a Polyvar Met microscope (PROFCONTROL GmbH) equipped with a Gryphax Altair camera (ENOPTIK AG) and analysis with the software IMAC IMS (IMAGIC Publigraphische Systeme). Scanning electron microscopy was performed using a Phenom XL (Fisher Scientific GmbH).

3 Results

3.1 Results of the mathematical analysis

The application of the methodology can be seen in Fig. 2, where part (a) shows the length change over the temperature

and (b) the first derivative v_s thereof. Figure 3 shows the second derivative a_s sorted by different heating rates and identical mechanical load and vice versa respectively, with the addition of the corresponding minima.

As shown in Fig. 2, the rate of deformation of the samples changes over the depicted temperature window. Figure 2a depicts a quasi-linear strain over the entire temperature window. As expected, higher applied stresses result in an overall slightly greater strain (linear elastic region). The almost linear appearance of the curve, with a slight trend upwards, is expected as the coefficient of thermal expansion α is only slightly positively temperature dependent ($\alpha_{150} = 12.5 \times 10^{-6}$ K^{-1} and $\alpha_{500} = 14.1 \times 10^{-6}$ K^{-1}). The slight decrease in Young's modulus E for higher temperatures should also cause a slightly positive slope (e.g., $E_{20°C} = 212$ GPa, $E_{400°C} = 184$ for 10CrMo9-10) [11]. The fast decline of the graph of the first derivative v_s (shown in Fig. 2b) and the increases in the graphs of Fig. 3a and b in the beginning until 100 °C are due to inaccurate measurements during the initiation phase. The steep incline of these graphs, above 400 °C, correlates directly with the applied stress and shows the beginning of necking. Much more interesting is the 100–350 °C zone in which the graph in Fig. 2b increases slightly until it reaches a local maximum. The specific temperature of the maximum is qualitatively between 250 and 350 °C, dependent on both the applied stress and the heating rate Φ. This means that the speed with which the testing area elongates rises. After that local maximum, the speed falls rapidly to a local minimum between 350 and 450 °C. This local minimum area was identified as "The Area of Interest." With respect to the here discussed experiment, a reduced velocity implies a higher deformation resistance, which in turn can lead to either increased localized stresses due to differences in thermal expansion of the different regions, or imply corresponding changes in hardness and toughness, or a combination thereof. These are important factors for the evaluation of the SRC susceptibility

Fig. 2 PWHT simulations for different heating rates and applied stresses on CGHAZ samples: **a** s-diagram over the temperature, **b** v_s diagram (first derivative)
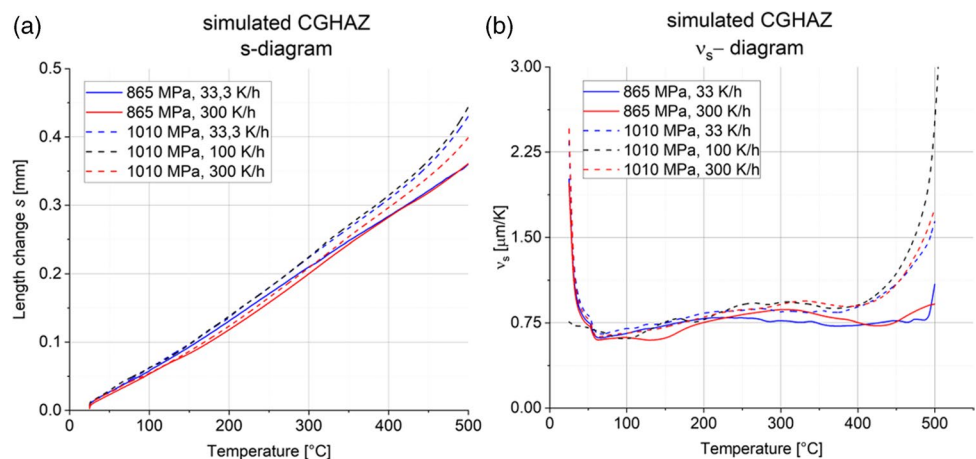
Fig. 3 a_s-diagram (second derivative) of PWHT simulations on CGHAZ samples: **a** effect of heating rate Φ at 1010 MPa, **b** effect of stress at $\Phi = 33$ K/h
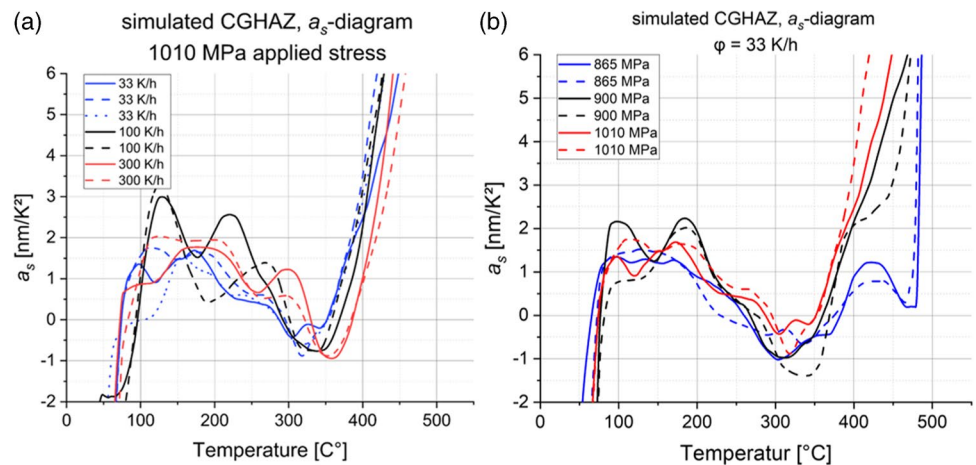
of 13CrMoV9-10. The CGHAZ exhibits a clear increase in hardness with the corresponding increase in tensile strength and decrease in deformation capacity.

To analyze the impact of the different heating rates Φ and applied stress level, the second derivatives in Fig. 3, Fig. 2a and b were used. The clear impact of the heating rate Φ can be seen in (a), where a higher heating rate correlates with the local minimum moved to higher temperatures. A significant difference of 40 °C between these two minima was observed. In practical terms, this means that the "maximum" resistance against deformation changes with higher heating rates Φ to higher temperatures. The effect of higher stresses was smaller than the effect of Φ. In Fig. 3b, the minima for different stress levels are closer together with 315 °C to 320 °C for $\Phi = 33.3$ K/h. Divergences in the local deformation capacity of the samples are clearly shown in Fig. 3, with a significant impact of Φ and to a lesser extent, for the stress levels as well.

To further validate the experimental methodology, identical comparative experiments were done for weld metal (WM) samples obtained from real welding experiments.

It must be stated that experimental results for the WM (selection shown in Fig. 4) exhibit a much larger spread for the elongation measurements compared to the simulated CGHAZ samples, which is due to the heterogeneous nature of a multi-pass weld and its derived samples. An overview of selected results for the WM is shown in Fig. 4 for 600 MPa and 900 MPa respectively. For both the WM and the base material, the here discussed characteristics and anomalies could not be shown (comprehensively in [12]). For the WM for example, the effect of a typical SAW multiple-pass weld promotes a reduction in hardness ([13, 14]), but the characteristic minimum in v_s and a_s of the CGHAZ between 300 and 350 °C, or at any other sensible temperature, could not be observed. This shows a very clear microstructural causation within the CGHAZ.

3.2 Microstructure correlation

The following scanning electron microscopy (SEM) visualization (Fig. 5) shows the side of a sample in the necking area. To ensure the crack initialization but not complete fracture break,

Fig. 4 PWHT simulations on weld metal samples: **a** v_s-Diagram weld metal, 600 MPa, **b** v_s-Diagram weld metal, 900 MPa
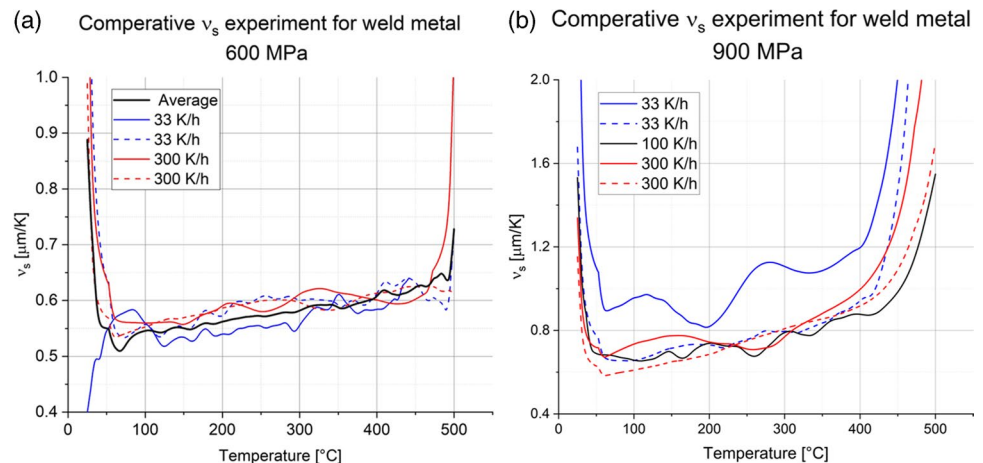
a stop parameter was programmed for individual experiments for specific heating rates and stress combinations. The trigger would stop the application of force when a defined (sudden) increase in the sample's elongation was detected.

The exemplary selected almost ruptured specimens in Fig. 5 visualize a Φ-dependent dissimilarity in the obtained fracture topography. For $\Phi = 33.3$ K/h, significant intergranular fracture was detected (part b)) as opposed to a larger ductile portion for $\Phi = 100$ K/h in part d of Fig. 5. The observed intergranular fracture indicates a higher SRC susceptibility for smaller heating rates, which was the working hypothesis. But this still tentative result must be evaluated critically because the observed intergranular topography is very localized. This method alone cannot be used as scientifically sound evidence of the impact of Φ. Especially the simulation of the impact of multiple-pass welds on the CGHAZ needs further study. But this alternative testing method provides clear benefits over other methods to evaluate SRC susceptibility, like hot tension tests with invariable temperatures. Additionally, proving the postulated cause of SRC, the effect of a dissimilar precipitation behavior dependent upon the present thermal and mechanical load via a microstructural analysis is non-trivial, if possible, at all. Effects like the carbide growth and formation could to date only be shown for higher temperatures and defined holding times [2, 13, 14]. Correlating a microstructural impact on the formation of microcracks in the CGHAZ, during the here discussed temperature window for samples heated to the typical 705 °C PWHT temperature, even without a dwell time, is all but impossible.

Microstructural analyses of the simulated CGHAZ samples after the specific PWHT cycle via scanning electron microscope (SEM) or even scanning transmission electron microscope (STEM) were unable to show discernable differences in microstructure due to different heating rates or applied force. STEM was used in Fig. 6a, b to depict CGHAZ samples after heating with $\Phi = 33$ K/h to 500 °C while 900 MPa was applied. Figure 6c and d shows samples heated with $\Phi = 300$ K/h to 500 °C with the same stress

applied via a uniaxial force. No clear differences could be identified between $\Phi = 33$ K/h and $\Phi = 300$ K/h. No microstructural differences due to different applied stresses during the PWHT via SEM or STEM were observed in similar experiments either. The reason for different SRC behavior of 13CrMoV9-10 for varied heating rates, and applied stresses are the formation and growth of precipitates due to elements formerly forced into solution ([15, 16]). These are highly localized and could not be directly observed in the inhomogeneous microstructure, especially due to the comparatively small observation window of STEM compared to the large sample diameter ([13, 14, 17, 18]).

Independent of the utilized heating rate and applied stresses over the cross section via a uniaxial tension force, the bainitic microstructure showed a high density of carbides and the typical elongated plate-like grains. Larger areas with very fine precipitates of high density within the grains were identified in all samples with no discernable differences due to the applied variables. Areas with needle-like carbides with similar orientation can be observed in all samples and are suspected to be cementite (Fe_3C). All samples presented with comparatively large carbides on the grain boundaries, which indicate Cr and Fe rich M_7C_3 carbides. These assertions were not able to be verified within the boundaries of this study. Multipass SAW-welds typically exhibit M_7C_3 and M_3C carbides as well as MX carbonitrides [17, 18]. Specifically, the microstructural analysis did not reveal any discernable impact of the heating rate or the applied stress on the microstructure or the size, density, or type of precipitation with this method.

3.3 Heating rate and stress-dependent, microstructure-specific hardness

In addition to the analytical methodology, a mechanical analog was investigated as a possible criterion for microstructural effects on a µm-scale (precipitates, grain boundaries etc.). For that reason, the hardness (HV0.5) was measured on a cross section of the WM of a real weld and on the simulated CGHAZ samples after their respective PWHT
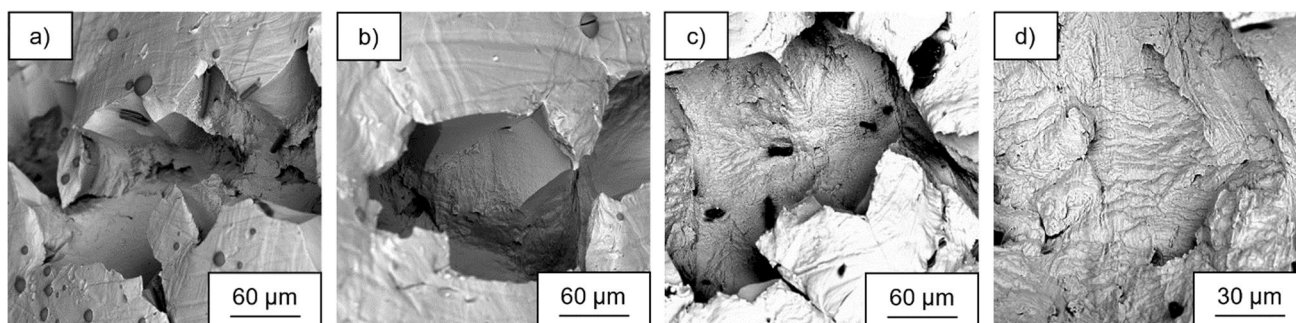

Fig. 5 SEM pictures of an initial fracture in the CGHAZ samples (1010 MPa load): **a** $\Phi = 33.3$ K/h (macro view) and **b** intergranular fracture (detail view); **c** $\Phi = 100$ K/h (macro view) and **d** dissimilar fracture topography mode (detail view)
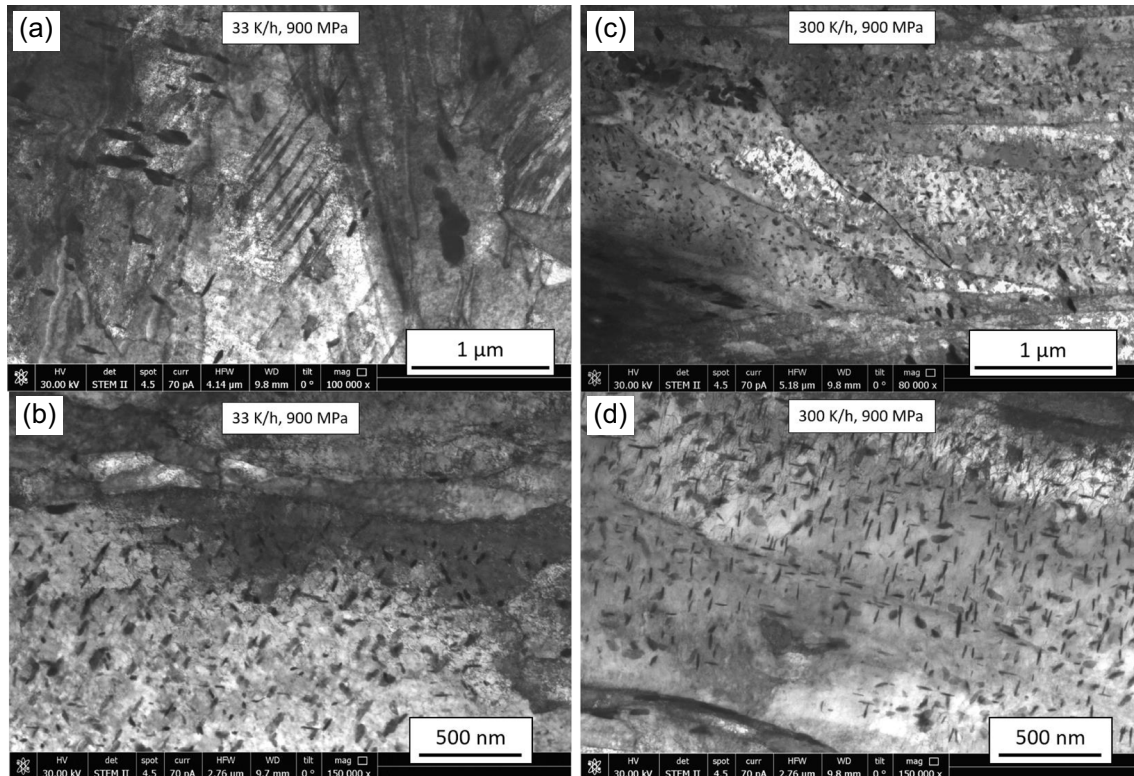
Fig. 6 Scanning transmission electron microscopy (STEM) comparison of simulated CGHAZ microstructures after different PWHT treatments: **a**, **b** $\Phi = 33$ K/h, $T_{end} = 500$ °C and 900 MPa, **c**, **d** $\Phi = 300$ K/h, $T_{end} = 500$ °C and 900 MPa

scenarios. Figure 7 shows the measured HV0.5 for different microstructures (WM, CGHAZ), heating rates, and applied stresses during the PWHT simulation. Different sample orientations were measured for the WM, with *L* denoting the lengthwise (along the weld seam) and *C* denoting the crosswise (perpendicular to the weld seam) orientation of the samples. The simulated CGHAZ samples show a significantly higher hardness in the reference case, without stress (dotted blue line), with 395 HV0.5. The lengthwise extracted WM (L) as well as the crosswise extracted WM (C) exhibit significantly lower values with 325 and 350 HV0.5 respectively. These differences are likely due to multipass welding SAW, which corresponds to a repeated partial heat treatment of the WM with a decreasing peak temperature per cycle (i.e., next welded layer) [2, 6, 14, 19]. For the here examined WM, no significant impact could be observed for the L- or C-samples with regard to the different heating rate and stress level combinations, as compared to the CGHAZ. The originally already high hardness of the CGHAZ, on the other hand, rises from 390 to 420 HV0.5. This high hardness and lowered ductility are reflected in the different fracture topography (intergranular fracture, Fig. 6). The presented methodology facilitates the systematic variation of applied stresses, during a simulated PWHT, with easily varied PWHT parameters such as heating rate or end/holding temperature with a
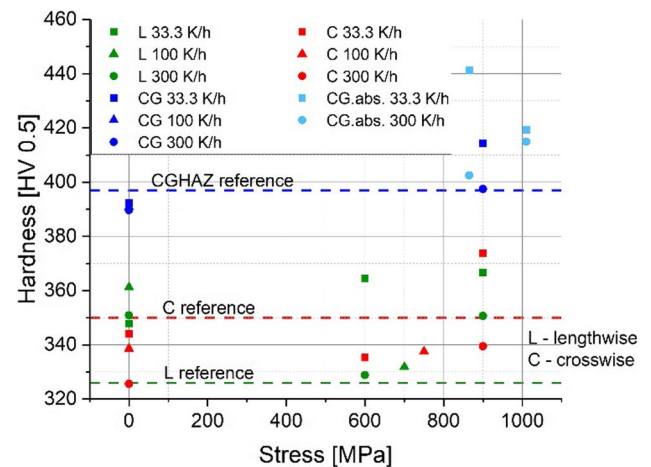
Fig. 7 HV0.5 hardness dependent on microstructure, heating rate, and applied stress

comparatively simple and easily adjusted experimental setup and the correlation to the HV0.5 hardness. Large thickness CrMoV welds generally exhibit very high residual stresses ([2, 20]), which can reach the yield strength of the specific CGHAZ or WM microstructure ([2, 5, 8, 20, 21]). This made the examination of very high test loads necessary.

4 Conclusions

Submerged arc welded creep-resistant steels with very large sheet thickness are susceptible to stress relief cracking if the mandatory PWHT is performed improperly or if the emerging mechanical loads during the welding and cooling process are insufficiently taken into consideration. Further research is currently being conducted, and the corresponding comprehensive results will be published in [22] among others. For the results of the proposed test methodology to identify SRC susceptibility shown here, the following conclusions can be drawn:

1. The developed test methodology enables the simultaneous physical simulation of PWHT cycles during a specified mechanical load especially of CGHAZ samples. These can be simulated in conjunction with the PWHT experiments, which allows for a streamlined workflow for these experiments. The defined mechanical load imitates and subsumes the higher residual stresses caused by the structurally induced stiffness of the surrounding construction including the not insignificant bending moments. The presented mathematical analysis via the first and second derivatives facilitates a fast and repeatable comparison between different experimental parameters.
2. A very clear microstructure dependency was observed, as the WM showed no reduction in velocity v_s during the PWHT. The property profile changes of different microstructures due to a possible precipitation influence are non-trivial to detect and are, at the time of publication, yet unclear. For that reason, the here discussed testing methodology allows for a robust but simplified evaluation of SRC susceptibility, utilizing a more realistic temperature and mechanical load profile.
3. The results of comparative hardness measurements show a correlation of increased hardness at lower heating rates Φ and movement of the minimum of the first and second derivatives of the length change to lower temperatures.
4. The findings of previous works [2, 5, 8, 20, 21] that the substitution of multiaxial stress distributions with a uniaxial tension stress requires extremely high stress levels (close to the respective yield strength of the CGHAZ and WM in the as-welded, hardened condition before the PWHT) to create SRC susceptible conditions were verified.

Declarations

Conflict of interest The authors declare no competing interests.

References

1. Hucinska J (2003) Advanced vanadium modified steels for high pressure hydrogen reactors. Adv Mater Sci 3:21–27
2. Lausch T (2015) Zum Einfluss der Wärmeführung auf die Rissbildung beim Spannungsarmglühen dickwandiger Bauteile aus 13CrMoV9–10, Bundesanstalt für Materialforschung und -prüfung (BAM), BAM-Dissertationsreihe 134
3. Tenckhoff E (1979) Zur Ursache der Rissbildung beim Spannungsarmglühen (stress relief cracking) in Wärmeeinflusszonen niedriglegierter Feinkornbaustähle. J Nucl Mater 82:239–256
4. Bentley K (1964) Precipitation during stress relief of welds in cr-mo-v steels (Crack formation during stress relief and welding in chromium-molybdenum-vanadium steels due to vanadium carbide precipitation). Br Weld J
5. Kromm ALT et al (2020) Influence of welding stresses on relief cracking during heat treatment of a creep-resistant 13CrMoV steel - part I: effect of heat control on welding stresses and stress relief cracking. Weld World 64:807–817
6. Boniszewski T (1972) Metallurgical aspects of reheat cracking of weldments in ferritic steels. Weld J 51:29–41
7. Rabe W (1974) Stand der Kenntnisse auf dem Gebiet der Versprödung geschweißter niedriglegierter Feinkorn-baustähle beim Spannungsarmglühen. Schweißen und Schneiden 26:386–389
8. Lausch T et al (2013) Schallemissionsmessung an Bauteilschweißungen aus 13CrMoV9–10 zum Nachweis von Spannungsrelaxationsrissen. Kolloquium Schallemission - Statusberichte zur Entwicklung und Anwendung der Schallemissionsanalyse 19
9. Schroepfer D, Kromm A et al (2021) Influence of welding stresses on relief cracking during heat treatment of a creep-resistant 13CrMoV steel - part III: assessment of residual stresses from small-scale to real component welds. Welding in the World 2021
10. Chabaud-Reytier M et al (2003) Mechanisms of stress relief cracking in titanium stabilised austenitic stainless steel. J Nucl Mater 323(1):123–137
11. Thyssenkrupp Werkstoffdatenblatt (2017) Legierter warmfester Stahl 10CrMo9–10. https://ucpcdn.thyssenkrupp.com/_legacy/UCPthyssenkruppBAMXJacobBek/assets.files/pdf/produkte/stahl-flachprodukte/werkstoffdatenblatt-10crmo9-10.pdf. Accessed 30 May 2023
12. Nietzke J (2021) Methodik zur Bewertung des Einflusses der mechanischen Beanspruchung auf SRC kriechfester Schweißverbindungen während des PWHT, Master thesis, Otto-von-Guericke Universität, Magdeburg, Germany
13. Schönmaier H, Fleißner-Rieger C, Krein R et al (2021) On the impact of post weld heat treatment on the microstructure and mechanical properties of creep resistant 2.25Cr–1Mo–0.25V weld metal. J Mater Sci 56(36):20208–20223

14. Schönmaier H et al (2020) Microstructural evolution of 2.25Cr-1Mo-0.25V submerged-arc weld metal. Weld World 64(2):379–393

15. Chen ZB et al (2017) Review of reheat crack in welded joint of low alloy heat-resistant steels. Key Eng Mater 730:15–20

16. Swift R (1971) The mechanism of stress relief cracking in 2–1/4cr-1mo steel. Weld J 50. http://files.aws.org/wj/supplement/WJ_1971_05_s195.pdf. Accessed 30 May 2023

17. Schönmaier H et al (2020) Continuous cooling transformation diagrams of 2.25Cr-1Mo-0.25V submerged-arc weld metal and base metal. Metals 10(8):1055

18. Schönmaier H et al (2021) Influence of the heat input on the dendritic solidification structure and the mechanical properties of 2.25Cr-1Mo-0.25V submerged-arc weld metal. J Mater Eng Perform 30(10):7138–7151

19. Fleißner-Rieger H et al (2021) On the impact of post weld heat treatment on the microstructure and mechanical properties of creep resistant 2.25Cr–1Mo–0.25V weld metal. J Mater Sci 56(36):20208–20223

20. Kromm A et al (2022) Influence of residual stresses on stress relief cracking of thick-walled creep resistant steel welds. International Conference on Residual Stresses ICRS-11. Nancy, Frankreich

21. Kromm ALT et al (2020) Influence of welding stresses on relief cracking during heat treatment of a creep-resistant 13CrMoV steel - part II: mechanisms of stress relief cracking during post weld heat treatment. Weld World 64:819–829

22. Czeskleba D et al (2022) Simulation einachsiger Spannungszustände in der Grobkornzone von UP-geschweißtem CrMoV-Stahl. DVS Berichte, Band 382